Long-term energy balance measurements at three different mountain permafrost sites in the Swiss Alps

Martin Hoelzle[1], Christian Hauck[1], Tamara Mathys[1], Jeannette Noetzli[2], Cécile Pellet[1], and Martin Scherler[1]

[1]Department of Geosciences, University of Fribourg, Fribourg, Switzerland
[2]WSL Institute for Snow and Avalanche Research SLF, Davos, Switzerland

Correspondence to: Martin Hoelzle (martin.hoelzle@unifr.ch)

Abstract. The surface energy balance is a key factor influencing the ground thermal regime. With ongoing climate change, it is crucial to understand the interactions of the individual heat fluxes at the surface and within the subsurface layers as well as their relative impacts on the permafrost thermal regime. A unique set of high-altitude meteorological measurements was analysed to determine the energy balance at three mountain permafrost sites in the Swiss Alps (Murtèl-Corvatsch, Schilthorn and Stockhorn), where data are being collected since the late 1990s in the framework of the Swiss Permafrost Monitoring Network (PERMOS). All stations are equipped with sensors for four-component radiation, air temperature, humidity, wind speed and direction as well as ground temperatures and snow height. The three sites differ considerably in their surface and ground material composition as well as their ground ice contents. The energy fluxes were calculated based on two decades of field measurements. While the determination of the radiation budget and the ground heat flux is comparatively straightforward (by the four-component radiation sensor and thermistor measurements within the boreholes), larger uncertainties exist for the determination of turbulent sensible and latent heat fluxes.

Our results show that mean air temperature at Murtèl-Corvatsch (1997 – 2018, 2600 m asl.) is -1.66 °C and has increased by about 0.8 °C during the measurement period. At the Schilthorn site (1999 – 2018, 2900 m asl.) a mean air temperature of -2.60 °C with a mean increase of 1.0 °C was measured. The Stockhorn site (2003 – 2018, 3400 m asl.) recorded lower air temperatures with a mean of -6.18 °C and an increase of 0.5 °C. Measured net radiation, as the most important energy input at the surface, shows substantial differences with mean values of 30.59 Wm^{-2} for Murtèl-Corvatsch, 32.40 Wm^{-2} for Schilthorn and 6.91 Wm^{-2} for Stockhorn. The calculated turbulent fluxes show values of around 7 to 13 Wm^{-2} using the Bowen ratio method and 3 to 15 Wm^{-2} using the bulk method at all sites. Large differences are observed regarding the energy used for melting of the snow cover: at Schilthorn a value of 8.46 Wm^{-2}, at Murtèl-Corvatsch of 4.17 Wm^{-2} and at Stockhorn of 2.26 Wm^{-2} is calculated reflecting the differences in snow height at the three sites.

In general, we found considerable differences in the energy fluxes at the different sites. These differences help to explain and interpret the causes to a warming atmosphere. We recognize a strong relation between the net radiation and the ground heat flux. Our results further demonstrate the importance of long-term monitoring to better understand the impacts of changes in the surface energy balance components on the permafrost thermal regime. The dataset presented can be used to improve permafrost

modelling studies aiming at e.g. advancing knowledge about permafrost thaw processes. The data presented and described here are available for download at the following site http://dx.doi.org/10.13093/permos-meteo-2021-01 (Hoelzle et al., 2021).

1 Introduction

High-mountain regions are particularly vulnerable to climate change (Haeberli and Beniston, 1998; Huggel et al., 2010, 2015; Pepin et al., 2022). Especially the alpine cryosphere, including the components snow, glaciers and permafrost, is reacting strongly to the ongoing atmospheric warming (IPCC, 2013; Hock et al., 2019). Significant changes in permafrost have already been documented by many observation networks world-wide (GCOS, 2010; Biskaborn et al., 2019; Noetzli et al., 2020; Smith et al., 2022). Operational mountain permafrost monitoring is particularly well established in Switzerland and include the longest mountain permafrost time series world-wide (Hoelzle et al., 2002), coordinated by the Swiss Permafrost Monitoring Network (e.g. PERMOS, 2019). As permafrost is not easily detectable from the surface (or space), it is investigated using temperature measurements in boreholes (Noetzli et al.) or non-invasive methods such as near-surface geophysics, which enable the analysis of the subsurface composition as well as the investigation of the ground ice content and its changes. Changes in ground ice content are important because they can be directly related to strong environmental impacts, such as the future development of natural hazard potential as well as changes in runoff amount and patterns, considerably affecting dry mountain regions (e.g. Walvoord and Kurylyk, 2016).

To better understand the complex process chains leading to the above mentioned impacts related to permafrost warming, we need to improve our knowledge about the thermal regime of permafrost, which is mainly determined by the energy balance at the surface and the geothermal heat flux at its lower boundary. The energy balance at the ground/snow surface is given by the net radiation, the turbulent heat fluxes, the melt energy of the snow cover, the heat flux through the snow cover and the ground heat flux. It has been subject of many field-based observational and modelling studies (e.g. Hoelzle and Gruber, 2008; Gruber and Hoelzle, 2008; Westermann et al., 2009; Langer et al., 2011a, b; Scherler et al., 2014; Chadburn et al., 2015; Marmy et al., 2016; Pellet et al., 2016).

It has to be noted that the permafrost thermal regime can vary substantially as a function of the surface cover. In coarse blocky terrain particular attention has to be given to the ground heat flux, as it can be very different from the mainly conductive heat flux in soil or bedrock substrates (e.g. Hanson and Hoelzle, 2004; Wicky and Hauck, 2017). Few studies have attempted to model heat transfer processes in such coarse blocky active layers by including e.g. turbulent heat fluxes within the active layer in their models (e.g. Scherler et al., 2014) or, more recently, air convection processes (e.g. Wicky and Hauck, 2017, 2020; Luethi et al., 2017; Pruessner et al., 2018).

However, in contrast to the above cited studies, most permafrost models use simpler formulations for the ground heat flux, and are based on estimations of the potential incoming radiation, modified by the effect of snow insulation (Etzelmüller, 2013; Riseborough et al., 2008). Other simplified approaches include thermal offsets which are calculated as the differences between air, surface and permafrost temperatures to characterize the influence of snow conditions and thermal conductivities of different

ground materials (Burn and Smith, 1988; Wu et al., 2003; Hoelzle and Gruber, 2008). In more recent permafrost or land surface models (e.g. Fiddes et al., 2015; Ekici et al., 2015; Pellet et al., 2016) the energy balance at the surface is explicitly included.

Nevertheless, only few observational datasets of the full energy balance at specific permafrost sites exist, especially in mountain regions. (Scherler et al., 2014; Boike and Abnizova; Boike et al.; Mohd Wani et al., 2020). The energy balance constitutes one of the most important input parameters for the ground heat flux regime, and it is therefore crucial to better understand the influence of the individual fluxes. Thus, such full energy balance datasets are necessary to improve the understanding and the ability to correctly model the various processes for different surface and subsurface materials in permafrost regions.

In this study, we focus on 20 years time series from three permafrost stations in the Swiss Alps (Schilthorn, Stockhorn and Murtèl-Corvatsch), which were established in the scope of the European research project PACE (Permafrost and Climate in Europe, (Harris et al., 2003; Etzelmüller et al., 2020)) at the beginning of this century and are now part of the PERMOS network. All stations are equipped with standard meteorological sensors such as a four component radiation sensor, air temperature, humidity, wind speed and direction as well as ground temperatures and snow height probes (Hoelzle and Gruber, 2008). All three sites differ considerably in their ground material composition and permafrost conditions. The influence of the radiation components and the turbulent heat fluxes on the ground heat fluxes and the snow melt energy is of particular importance for high mountain permafrost research as they determine the ground thermal regime in the first place and therefore also the geotechnical behaviour of the permafrost. The main aims of this paper are the following: (1) to present a long-term dataset of meteorological measurements at three different mountain permafrost sites and make this dataset available to national and international databases; (2) to quantify the energy fluxes at the surface of these permafrost sites using the long-term datasets; (3) to record and explain patterns of variation in surface layer meteorology for the different surfaces and to compare them. These objectives are important for the development of physically based energy balance models for permafrost environments and to evaluate their sensitivity to climatic warming.

2 Study sites and measurements

All three investigation sites, Schilthorn, Stockhorn and Murtèl–Corvatsch are characterized by the occurrence of deep-seated permafrost, which is currently warming at a high rate. This is shown in Figure 1, where the temporal evolution of the ground temperatures in the boreholes are plotted. The measurement sites were initially instrumented for research purposes and not as long-term monitoring stations; the data have some larger gaps, which could only partly be filled. Details to the individual measurements at each location can be found in Hoelzle and Gruber (2008) and table 1. Raw measurements mainly consist of 10 minute values, which were averaged and stored as hourly means. The data are stored in Campbell loggers (CR10X or CR1000) and are directly transferred via GSM communication to the PERMOS database.

2.1 Murtèl–Corvatsch

The Murtèl–Corvatsch area is situated in the Upper Engadine (Eastern Swiss Alps). A steep NW-facing rock wall surrounds the area and the slopes below the rock walls are covered by several meters of loose debris. Several rockglaciers and protalus

ramparts are situated at the foot of the rock wall. One of these rockglaciers is the Murtèl rockglacier, which has been investigated for more than 30 years (Hoelzle et al., 2002). It consists of a coarse blocky surface layer with a thickness of about 3 - 6 m above an ice supersaturated permafrost layer of about 25 m thickness, followed by a thick layer of undersaturated blocks. The rocks consist of deeply weathered micaceous shales. The mean annual precipitation sum (1981-2010) measured at the nearby station of MeteoSwiss at Sils-Maria is 1011 mm whereas about 1295 mm were recorded on the Piz Corvatsch summit station. A first borehole was drilled in 1987 and has continuously provided ground temperature data. This borehole was replaced by a new one in 2015 (PERMOS, 2019). In 1997, a first micrometeorological station was installed at this site (Mittaz et al., 2000). The station is at around 5 m distance from the boreholes. Air temperature, air humidity, radiation (all components), surface temperature, snow depth, wind speed and wind direction are measured at around 2 m above ground (Hoelzle and Gruber, 2008).

2.2 Schilthorn

The Schilthorn is situated at the transition between the Prealps in the north and the principle chain of the Bernese Alps (Northern Swiss Alps), which exceed 4000 m a.s.l. Due to its geographic situation (exposed to moist western winds), the climate in the Schilthorn massif is of suboceanic alpine character, i.e. with fairly abundant precipitation, showing a distinct summer maximum. The mean annual sum in Lauterbrunnen (valley floor) is 1234 mm whereas about 2700 mm were estimated on the highest summits, where about 90% of the precipitation falls as snow. As a consequence, the surface is snow-covered for longer periods than in most regions with the same elevation in comparison to the central Alps. The Northern slope of the Schilthorn summit, where the micrometeorological station was installed in 1998, is covered by a few metres of fine grained debris of sandy and silty material with a low ice content (Imhof et al., 2000). The station was installed on a small plateau at 2900 m a.s.l. Air temperature, air humidity, radiation (all components), snow depth, wind speed and wind direction are measured at around 2 m above ground (Hoelzle and Gruber, 2008). In the same year, a 14-m deep borehole was drilled into bedrock a few meters to the northwest of the climate station and equipped with a thermistor chain. Two additional boreholes were drilled in 2000: a vertical one having a depth of 100 m and one perpendicular to the surface with a depth of 92 m. A 20m deep replacement borehole was drilled in 2018 at a few meters distance to the boreholes drilled in 2000. In addition, soil moisture data are recorded nearby (Pellet and Hauck, 2017).

2.3 Stockhorn

This study site is located in the upper Mattertal/Walliser Alpen in the Southern Swiss Alps. The station is located on a mountain ridge which extends from the Gornergrat to the Stockhorn mountain summit. The station is situated at an altitude of 3410 m a.s.l. on a small plateau which is gently inclined to the south (45°59'N, 7°49'E). Surface conditions are heterogeneous with medium-size debris, fine grained material and outcropping bedrock and intermediate ice contents. The bedrock belongs to the palaeozoic crystalline Monte Rosa nappe and consists on Albit-Muskovit schists. At some places the development of patterned ground is visible, especially where the station is located. The Stockhorn–Gornergrat crest is surrounded by mountain ranges that exceed altitudes of 4000 m a.s.l. This causes a local climate characterized by reduced cloud cover and high solar radiation.

The annual precipitation in the Zermatt valley is relatively low with 639 mm according to the MeteoSwiss for the period 1981 – 2010 and can be estimated to be around 1500 mm at Stockhorn based on King (1990). Two boreholes were drilled in 2000. One borehole is 100 m deep and is located on the plateau, whereas a second borehole is 31 m deep and situated around 25 m to the south close to the edge of the plateau. A meteorological station was installed in 2002 close to the deep borehole. Air temperature, air humidity, radiation (all components), surface temperature, snow depth, wind speed and wind direction are measured at around 2 m above ground (Hoelzle and Gruber, 2008). In addition, soil moisture data are recorded nearby (Pellet and Hauck, 2017).

3 Methods

3.1 Calculation of the Surface Energy Balance

The energy balance at the surface can be formulated as follows (energy fluxes are in units of Wm^{-2} and positive when directed towards the surface):

$$Q_{SW}\downarrow + Q_{SW}\uparrow + Q_L\downarrow + Q_L\uparrow + Q_H + Q_{LE} + Q_S + Q_P + Q_G + Q_M = 0 \tag{1}$$

where $Q_{SW}\downarrow$, $Q_{SW}\uparrow$ are the shortwave incoming and reflected radiation, $Q_L\downarrow$ and $Q_L\uparrow$ are the longwave incoming and emitted radiation fluxes, Q_H is the turbulent sensible heat flux, Q_{LE} is the turbulent latent heat flux, Q_S is the heat flux through the snow cover, Q_P is the sensible heat energy supplied or consumed by precipitation falling on the surface. It is ignored as it is in general negligibly small compared with the other fluxes (Brock et al., 2010). Q_G is the heat flux in the ground and Q_M denotes snow melt at the surface.

3.1.1 Short- and longwave radiation fluxes

$Q_{SW}\downarrow$, $Q_{SW}\uparrow$, $Q_L\downarrow$, $Q_L\uparrow$ were measured directly at the individual meteostations using a CNR1-device at each of the three sites (for further details see table 1). The sensors were relatively reliable during the measurement period and only a few longer gaps occurred. The sum of all radiation components is called the net radiation Q_R. It is a fundamental factor for all energy balance studies as it typically is the component with the highest energy gain or loss.

3.1.2 Turbulent sensible and latent heat flux

The turbulent fluxes were calculated using two methods a) the bulk aerodynamic method (e.g. Munro, 1989; Denby and Greuell, 2000; Arck and Scherrer, 2001; Oke, 1987) and b) the Bowen ratio method (Bowen, 1926).

3.1.3 Bulk method

Knowing that turbulent sensible and latent heat fluxes over rock and debris surfaces cannot be estimated using neutral stability assumptions (Nakawo and Young, 1982; Mattson and Gardner, 1989; Takeuchi et al., 2000; Nicholson and Benn, 2006), it is

necessary to apply corrections for non-neutral conditions due to the large variations in atmospheric stability. The stability of the atmospheric layer close to the surface can be described by the bulk Richardson number, Ri_b , relating the relative effects of buoyancy to mechanical forces (Brutsaert, 1982; Moore, 1983):

$$Ri_b = \frac{g(T_a - T_s)(z - z_{0m})}{T_0 u^2} \tag{2}$$

5   where g is the acceleration due to gravity ($9.81 ms^{-2}$); T_0 is the average of air temperature (T_a) and the surface temperature (T_s); z_{0m} is the surface roughness length for momentum taken from Brock et al. (2006, 2010) as 0.016 and 0.001 for snow free and snow covered conditions, respectively; T_a is the air temperature; T_s is the surface temperature and u is the wind speed measured at the station. Stability corrections based on Ri_b have been applied successfully over rockglaciers (Mittaz et al., 2000). Assuming that the local gradients of mean u , mean T and mean specific humidity q are equal to the finite differences

10 between the measurement level and the surface, the turbulent fluxes may be evaluated as follows (after Brutsaert (1982); Favier et al. (2004); Sicart et al. (2005)):

$$Q_H = \rho_a \frac{c_p k^2 u(T_a - T_s)}{(ln\frac{z}{z_{0m}})(ln\frac{z}{z_{0t}})} (\phi_m \phi_h)^{-1} \tag{3}$$

$$Q_{LE} = \rho_a \frac{L_v k^2 u(q_a - q_s)}{(ln\frac{z}{z_{0m}})(ln\frac{z}{z_{0q}})} (\phi_m \phi_v)^{-1} \tag{4}$$

     where q_a and q_s are specific humidities ($kg kg^{-1}$) at the 2 m and surface levels, respectively; ρ_a is the air density; c_p is

15 the specific heat capacity for air at constant pressure ($c_p = c_{pd}(1 + 0.84q)$ with $c_{pd} = 1005 J kg^{-1} K^{-1}$); k is von Karmans constant ($k = 0.4$) and L_v is the latent heat of vaporisation ($L_v = 2.476 * 10^6 J kg^{-1}$ at 283 K). The scalar lengths for heat z_{0t} and humidity z_{0q} were considered to be equal to z_{0m}. ϕ_m, ϕ_h, ϕ_v are the non-dimensional stability functions for momentum, heat and moisture, respectively and they are unity in neutral cases. They are expressed as functions of Ri_b for stable and unstable cases:

20   Stable case ($0 < Ri_b < 0.2$):

$$(\phi_m \phi_h)^{-1} = (\phi_m \phi_v)^{-1} = (1 - 5Ri_b)^2 \tag{5}$$

     Unstable case ($Ri_b < 0$):

$$(\phi_m \phi_h)^{-1} = (\phi_m \phi_v)^{-1} = (1 - 16Ri_b)^{0.75} \tag{6}$$

3.1.4   Bowen ratio method

25 The Bowen ratio method estimates the sensible and latent heat fluxes Q_H and Q_{LE} according to the energy available (e.g. $Q_R + Q_G + Q_M + Q_S$). The energy partitioning between Q_H and Q_{LE} has direct relation to the boundary-layer climate and

is called Bowen ratio β (Bowen, 1926):

$$\beta = \frac{Q_H}{Q_{LE}} = \frac{c_p(T_a - T_s)}{L_v(q_a - q_s)} \tag{7}$$

with

$$Q_H = \frac{Q_R + Q_S + Q_G + Q_M}{1 + \frac{1}{\beta}} \tag{8}$$

and

$$Q_{LE} = \frac{Q_R + Q_S + Q_G + Q_M}{1 + \beta} \tag{9}$$

Using the Bowen ratio energy-balance method leads to some uncertainties, which has to be taken into account when interpreting the data. First, errors of net radiation and subsurface fluxes are accumulated in the evaluation of the turbulent fluxes. Secondly, the Bowen ratio method often produces non-physical sensible and latent heat fluxes: wrong signs (directions) and extremely large magnitudes of the fluxes. Therefore, we follow a procedure proposed by Ohmura (1982) using two criteria for rejecting such undesirable data. The first criteria is defined by the condition that data are excluded, if the conditions below are not met:

if $Q_R + Q_G > 0$ then $\Delta T > (-L_v/c_p)\Delta q$

if $Q_R + Q_G < 0$ then $\Delta T < (-L_v/c_p)\Delta q$

The second criteria is defined by the necessary condition that the denominator in the equations and cannot be zero. This case occurs when $\beta = -1$. In order to consider the accuracy of temperature and specific humidity, this condition is formulated as follows:

$\Delta T > -(L_v/c_p)\Delta q - 2[(L_v/c_p)E(q) + E(T)]$

$\Delta T < -(L_v/c_p)\Delta q + 2[(L_v/c_p)E(q) + E(T)]$

where E_T and E_q are the resolution limits of the thermometer or the hygrometer.

3.1.5 Snow heat flux

The snow heat flux is given by

$$Q_S = -k_{snow}\frac{dT}{dz} \tag{10}$$

where, according to (Keller, 1994; Mellor, 1977), the heat conductivity of snow $(Wm^{-1}K^{-1})$ is determined by $k_{snow} = 2.93(\rho_{snow}^2 10^{-6} + 0.01)$. Snow density ρ_{snow} was fixed to a value of $220\ kgm^{-3}$. Typical values for k_{snow} lie between 0.2 and 0.5 $(Wm^{-1}K^{-1})$ (e.g. Sturm et al., 1997; Essery et al., 2013). Due to these low values, the transport of heat through the snow cover is generally small. Hence, snow insulates the ground from atmospheric influences.

3.1.6 Ground heat flux

While the ground surface temperature is a function of the varying energy-exchange processes at the atmosphere/lithosphere boundary, their downward propagation depends on the thermal properties of the ground (Williams and Smith, 1989). Heat conduction is the main process of heat transfer within the ground when considering the ground as a homogeneous medium. In addition, heat transport takes place by circulation of water and convective and advective circulation of air. However, these processes are not included in the calculations to keep the approach as simple as possible:

$$Q_G = -k(\Delta T/\Delta z) \tag{11}$$

where Q_G = ground heat flux and k = thermal conductivity of the ground in $Wm^{-1}K^{-1}$.

3.1.7 Snow melt

The energy provided by snow melt is

$$Q_M = L_M R_S \tag{12}$$

where L_M = latent heat of fusion for ice ($336 kJkg^{-1}$). The runoff rate R_S can be obtained as a function of the change of the product of snow height h and snow density ρ_s, which was fixed to a value of 220 kgm^{-3}:

$$R_S = \frac{\Delta(\rho_{snow}h)}{\Delta t} \tag{13}$$

3.2 Data processing

As the monitoring evolved slowly from individual research projects (e.g. PACE) into the long-term PERMOS monitoring, the data availability is relatively poor. At the beginning of the observation period at all three stations major data gaps up to several months exist for all measured variables. For air temperature and snow height, being the most important meteorological variables for many permafrost modelling studies, an almost complete time series was generated by gap filling using complementary information from nearby meteorological stations (mainly based on Intercantonal Measurement and Information System (IMIS) or MeteoSwiss (MCH) stations). For the energy balance calculation, only shorter gaps were filled using correlations between the individual variables at the stations itself to guarantee that the energy balance is based on in-situ data gathered at the meteorological stations alone.

Several data sets are prepared for this study, which are classified into three levels. Level 0 is the collected set of raw data, mainly obtained directly from the loggers (wherever the data were still available). These data are not treated at all and large part of the data set may contain errors. Level 1 data consist of corrected and partly gap-filled data. The gap filling process is described below. Finally, level 2 data are the final data set, including additional data processing steps such as correction of shortwave incoming radiation due to snow covered sensors. For further studies, the use of the level 2 data set is recommended. The raw data (level 0) were processed using the following processing steps:

- range check and small corrections (level 1): For all stations, the data of the variable **air temperature** outside the range of –40 to +30 °C and **relative humidity** data outside the range of $0 - 101$ % were deleted. Data between 100 and 100.9 % were corrected to 100 %. **Snow height** data were corrected after comparison with neighbouring operational stations in the close surroundings of Murtèl-Corvatsch, Schilthorn and Stockhorn. Individual outliers were either deleted or corrected manually with the help of additional information from our station measurements such as albedo. Negative incoming and outgoing **shortwave radiation** during the night were set to 0. Unrealistically high values (> than top of atmosphere radiation, 1366 Wm^{-2}) were corrected to a value corresponding to its neighbouring values. For the level 1 data, no correction was made for snow coverage on the sensor.

- short gap filling (level 1): In general, single missing values for up to three hours were corrected by taking the preceding value to fill the unknown values. By this, air temperature and snow height data were almost completely gap-filled. All hourly data gaps for Schilthorn snow height were filled and only 0.0039% data gaps for air temperatures remain. At Stockhorn 4.99% of data gaps are still present after the gap filling in both snow heigt and air temperature data and for Murtél-Corvatsch 0.1% for snow height and 2.31% for air temperature remain.

  In addition, site specific processing steps were performed for the different variables.

- long gap filling (level 1): For data gaps larger than 3 hours, missing values were filled using linear regression between data from nearby stations or the station itself. The corresponding variables and coefficients of the linear regressions can be found in table 2. **Snow height** data at the Murtél-Corvatsch station were corrected by taking the snow height data from the station Lagrev IMIS with a multiplication factor of 0.625. In the case of Schilthorn the station Türliboden IMIS with a factor of 0.58016 and for Stockhorn the station Gornergrat IMIS with a multiplier of 0.369425 were used.

- radiation corrections (level 2): Level 2 data were corrected using α (albedo) for fresh snow (α = 0.87, (Oke, 1987)) and multiplying it with outgoing radiation. **Longwave incoming radiation** was additionally corrected for the known influence of the shortwave incoming radiation by using the formula given by Sicart et al. (2005) $Q_L\downarrow = Q_L\downarrow$ - (corr * $Q_{SW}\downarrow$), where corr is equal to 2%. We considered also that the radiation input perpendicular to a slope is decisive for the energy balance of a surface. The values obtained for the different radiation components have, therefore, to be adapted to the local slope. As a consequence, the values at Murtél-Corvatsch (local slope is 2°) and at Schilthorn (local slope is 7°) were corrected by dividing the obtained measurement values with the cosine of this angle.

- data aggregation: First, the data were corrected and stored as level 1 hourly data. Then the radiation corrections mentioned above were applied to produce level 2 data. From the level 2 data, the energy balance was calculated. Following a recommendation by the WMO (2017), mean daily values were then calculated from the hourly values if at least 19 hours of data were available for a full day. From the daily values, we calculated monthly mean values using a threshold of 25 days meaning that monthly means are only calculated when at least 25 days of a month were available.

A special case is the Stockhorn station, where meteorological data between 2002 and 2006 were only stored as six hourly mean values, with frequent data gaps. Therefore, energy balance was only calculated for the period 2006-2018, after the station

was reprogrammed to record hourly values. Level 2 data could only be produced for this time period. Nevertheless, level 1 daily meteorological data for Stockhorn were produced for the whole period since 2002, albeit with reduced data quality.

4   Results

We will provide some of the long-term time series, which are of relevance for the permafrost monitoring such as the air temperatures, snow heights or also information about the dates of the first larger snow fall and snow melt out. We will mainly present monthly aggregated values of all meteorological variables as well as of the individual energy balance components.

4.1   Measured meteorological components at the three sites

Figure 2 shows the evolution of the mean daily air temperature, snow depth and ground temperatures at all three sites. The observed mean air temperature for the individual observation periods are -1.66 °C at Murtèl-Corvatsch (1997—2018), at Schilthorn (1999—2018) -2.60 °C and at Stockhorn (2003–2018) -6.18 °C. During the observation periods the measured air temperatures show a warming of 0.8 °C at Murtèl-Corvatsch, 1.0 °C at Schilthorn and 0.5 °C at Stockhorn. Measured mean snow heights (Figure 2) for the winter periods results in 0.50 m at Murtèl-Corvatsch, 0.87 m at Schilthorn and 0.32 m at Stockhorn. Snow height at Schilthorn is close to three times the value of Stockhorn. Absolut maximum snow height for Murtèl-Corvatsch is 2.27 m, for Schilthorn 4.01 m and for Stockhorn 2.11 m. The mean of annual maximum snow height for for Murtèl-Corvatsch is 0.53 m, for Schilthorn 0.88 m and for Stockhorn 0.31 m. A slightly increasing trend of snow height during the observation periods is recorded at the Murtèl-Corvatsch and Stockhorn sites and a decreasing trend is observed at the Schilthorn site (trends using Mann-Kendall and Sen-slope are not significant). However, the trend would also be positive when the first winter in 1999 with a record snow height would be neglected. The dates when the snow cover starts to build up in autumn and when the snow melt is completed in spring was determined from the snow height sensor resulting in the amount of snow free days. Figure 3 illustrates that the number of snow free days during the observation periods have an increasing tendency. However, using the Mann-Kendall test, only for Schilthorn a statistically increasing trend was calculated. The evolution of the near surface ground temperatures measured in the boreholes is shown in Figure 2. The mean ground temperatures are slightly negative for Stockhorn with -0.43 °C at a depth of 0.3 m and -0.32 °C at 0.8 m, but positive for Schilthorn (0.03 °C at a depth of 0.2 m and 0.04 °C at 0.4 m) and Murtèl-Corvatsch (0.07 at a depth of 0.5 m and -0.28 °C at 1.5 m). This reveals that the observed permafrost at lower depths at these sites is either not in equilibrium or that other processes in the active layer produce a considerable offset, as it is the case at the Murtèl-Corvatsch site with the coarse blocky surface (Hanson and Hoelzle, 2004; Scherler et al., 2014).

The shortwave incoming and outgoing radiation show mean values of 147.91 Wm^{-2} and -71.50 Wm^{-2} for Murtèl-Corvatsch, 149.61 Wm^{-2} and -75.87 Wm^{-2} for Schilthorn and 209.69 Wm^{-2} and -131.32 Wm^{-2} for Stockhorn, respectively, resulting in mean albedo values of 0.48 for Murtèl-Corvatsch, 0.51 for Schilthorn and 0.63 for Stockhorn. For the longwave incoming and outgoing radiation the following values were observed, 254.40 Wm^{-2} and -300.38 Wm^{-2} for Murtèl-Corvatsch, 254.97 Wm^{-2} and -296.02 Wm^{-2} for Schilthorn and 213.35 Wm^{-2} and -284.78 Wm^{-2} for Stockhorn,

respectively (see Figure 4 and table 3). The corresponding net shortwave and longwave radiation are 76.41 Wm^{-2} and -45.41 Wm^{-2} for Murtèl-Corvatsch, 73.34 Wm^{-2} and -41.05 Wm^{-2} for Schilthorn and 78.37 Wm^{-2} and -71.43 Wm^{-2} for Stockhorn (see Figure 4 and table 3). At Murtèl and Stockhorn, the radiation components show a slight decreasing trend of incoming shortwave radiation and an increasing trend for incoming longwave radiation - except for the Schilthorn site (Nyeki et al., 2019). At all sites the mean observed relative humidity is close to 70% and shows a clear seasonal behaviour with monthly values close to 60% during winter and around 80% during summer. We observe that at Murtèl-Corvatsch the wind speed has a mean value of 1.69 ms^{-1}, which is much lower than at Schilthorn with a mean wind speed of 1.97 ms^{-1} or Stockhorn with 2.09 ms^{-1} (see table 3). Wind direction at Murtèl-Corvatsch and Schilthorn are particularly influenced by topography as both stations are located on Northern exposition and are influenced by mountain crests to the South. The Stockhorn station is situated on a mountain crest with dominant wind direction from East-Southeast (Figure 5).

4.2 Energy Balance

The energy balance at the surface is particularly important as it defines the boundary conditions for the energy transfer between the atmosphere and the subsurface. It has major impacts on the ground heat flux and on the occurrence of permafrost. The components of the energy balance at Stockhorn are smaller than at the other two sites (Figure 6). The partitioning of the energy balance components is of particular interest. At all three sites the most important energy balance component is the net radiation, which has a net positive value (see Figure 6). Net radiation is only about 20% of the net radiation at Schilthorn and Murtèl-Corvatsch. The monthly values show strong seasonal fluctuations (Figure 7). At Stockhorn, the net radiation is negative from October to April whereas at Schilthorn and Murtèl-Corvatsch, it is only negative between November and February (Figure 7). The influence of the snow cover on the energy fluxes is of very high importance. Particularly in spring, snow is using the whole energy of the incoming shortwave radiation to be melted and large differences are occurring for the energy transfer if the ground is snow covered or not. We can see a strong difference between the sites. Schilthorn generally has a thick snow cover and in the months of April to July much of the available energy is used for its melting (mean value of 8.46 Wm^{-2}, Figure 6, table 4), which is much more than at the other two sites which show mean values of 2.26 Wm^{-2} at Stockhorn and 4.17 Wm^{-2} at Murtél-Corvatsch (Figure 6, table 4).

The results for the three sites show that the turbulent fluxes vary between 6 to 15 Wm^{-2} using the Bowen ratio method and between 3 to 15 Wm^{-2} using the bulk method (table 4). The results of both methods correlate relatively well with coefficients of determination (r^2) between 0.5 and 0.7. In comparison to the other fluxes, the heat fluxes in the snow and in the ground are very small with mean values lower than 1 Wm^{-2} (Figure 6, table 4).

5 Discussion

All three stations show a clear atmospheric warming trend. However, the warming is different at all stations. At Schilthorn (period 1999 – 2018), we see the strongest increase in air temperature with around 0.054 $°Cyr^{-1}$, whereas Murtèl-Corvatsch (period 1997 – 2018) and Stockhorn (period 2003 – 2018) experience a smaller air temperature increase with 0.038 $°Cyr^{-1}$

and $0.036\,^{\circ}Cyr^{-1}$. However, the temperature increase is different when only considering a period where data are available from all three stations. Taking into account only the observation period $2003 - 2018$, the trend changes particularly at the Murtèl-Corvatsch site with an increase of $0.073\,^{\circ}Cyr^{-1}$. For the same period, Schilthorn recorded a temperature increase of $0.057\,^{\circ}Cyr^{-1}$. The temperature rise is slightly higher when compared to the observed decadal increases between $1991 - 2020$
5 determined regionally by MeteoSwiss, but our observations are only covering the last two decades, where the atmospheric warming was most pronounced.

    An interesting fact is a decrease in shortwave incoming radiation observed at all sites, most pronounced at Schilthorn. We cannot explicitly explain this observation, but it might well be related to an increase in cloudiness. The melt energy used during the spring season at all three sites seems to be of great importance. The large temporal variability of the snow cover
10 at the individual sites and the large topographical differences between them are considerable. Schilthorn shows the thickest and longest-lasting snow cover during the observation period and its isolating effect and its energy sink function during melt is probably key to keeping permafrost conditions active at this site. If the number of snow days in spring and early summer decreases (as projected under future climate scenarios, (Scherler et al., 2013; Marmy et al., 2016), then the absorbed heat at the surface will increase with a corresponding increase of ground heat flux downward. We can estimate this potential increase
15 if we compare the observed July ($11.51\ Wm^{-2}$) or August ($8.32\ Wm^{-2}$) ground heat flux with the ground heat flux of May ($0.98\ Wm^{-2}$) and June ($4.28\ Wm^{-2}$). These estimates are partly confirmed by the observed increase of Q_G downwards into the ground, particularly at Murtèl-Corvatsch and Schilthorn for June and at Stockhorn for May (Figure 8). An increasing trend of snow free days has already been observed and is pointing to a corresponding change of the heat fluxes within the last two decades (see Figure 3).

20   Furthermore, clear differences in the radiation components at the three sites can be seen. Stockhorn is situated at higher elevation and the recorded observations show lower air temperatures as well as correspondingly lower incoming longwave radiation (Figure 6). However, shortwave incoming radiation is much higher in contrast to the other two sites leading to a higher relative importance of the shortwave incoming radiation on the energy balance at Stockhorn (Figure 6). At higher altitudes, in general higher amounts of solar radiation and higher insolation variability are observed than at lower altitudes. In
25 addition, Stockhorn is a relatively dry location with lower humidity and correspondingly lower cloudiness. These observations are of particular interest for the question of elevation dependent warming (EDW) (Wang et al., 2016; Pepin et al., 2015). As stated in Pepin et al. (2015), a combination of mechanisms are probably responsible for the more pronounced warming trends observed at high altitude stations: (i) the albedo feedback due to retreating snowlines (e.g. Scherrer et al., 2012), (ii) the cloud feedback caused by increased latent heat release (Ohmura, 2012), and (iii) the water vapour-radiative feedbacks,
30 which is impacting the relationships between longwave radiation, moisture and thermal regimes and are particularly enhanced at low temperatures where already small amounts of water vapour increase can lead to a substantial influence on the incoming longwave radiation (Pepin et al., 2015). In addition to the feedback mechanisms mentioned above, the relationship between temperature and outgoing longwave radiation is a consequence of the blackbody emission, which is proportional to the fourth power of temperature (Stefan–Boltzmann law). Therefore, if the outgoing longwave radiation is increasing, a larger temperature
35 change at lower temperatures will result.

The albedo feedback, observed at all three sites as the number of days without snow is strongly increasing. Regarding the cloud feedback, we find evidence for this effect at all stations by the above mentioned observation of reduced shortwave incoming radiation and increased temperatures. This may be the most important factor for the strong warming observed at the Schilthorn site. The water vapour-radiative feedbacks may also explain the observed difference between the comparatively dry Stockhorn and the other sites related to the stronger ground temperature increase. However, the overall resulting response at the individual sites is complex and the above mentioned effects will impact the different sites with different magnitude. For a better understanding, the presented data from the three stations should be combined with data from other stations in the Alps to gain a better understanding of the effects of EDW.

A significant result of this study is depicting the high dependency of the ground heat flux on the net radiation (see Figure 9). It is especially interesting that a single linear relation from net radiation can be used to calculate the ground heat flux at all three stations with reasonable accuracy. We want to point to the fact that it could be of special interest for the development of simplified permafrost distribution models based on easy to calculate input parameters. In this case a rough land classification in combination with the calculated radiation fluxes would allow to use the relation shown in Figure 9. It could also be shown that the air temperature is another important factor for the ground heat flux, which is clearly visible in Figure 10. However, it has to be noted that the linear relations show different slopes which do not allow for a universal application to a larger region as the individual relations at each station have to be taken into account.

Finally, thermal offsets relate the air temperatures to the ground temperatures, which is of relevance in most atmosphere–permafrost investigations. In this study, we observe a very large offset at Stockhorn when compared to the other two sites (see Figure 11). In general, the thermal offset is strongly influenced by the snow cover and by the amount of incoming shortwave and longwave radiation. The meteorological observations at the three sites revealed that the Stockhorn site receives more incoming shortwave than longwave radiation in comparison to Schilthorn and Murtél-Corvatsch. As shortwave radiation has a pronounced impact on the surface temperature and subsequently also on the ground temperatures while the ground is snowfree, the resulting thermal offset is larger at this site with higher shortwave radiation compared to sites where the air temperature and the corresponding incoming longwave radiation are dominant in the energy balance. This type of observations related to the thermal offset of different sites could also be detected along a latitudinal transect from the Arctic to Alps showing a higher thermal offset in the Alps than in the Arctic (Etzelmüller et al., 2020), which seems to be influenced by the same conditions such as a thicker snow cover and stronger incoming shortwave radiation.

6 Conclusions

We compiled, processed and quality checked the long-term meteorological data sets from three high mountain permafrost stations in the Swiss Alps by means of basic criteria. All three sites are embedded in the Swiss Permafrost Monitoring Network. The meteorological measurements cover a period of about two decades. The collected data provide valuable information allowing an in depth insight into the surface energy exchange processes at the different permafrost observation sites. This clearly shows the advantage of long-term monitoring stations in comparison to only short-term project based observations

where certain long-term trends and changes cannot be detected. The data are freely available for all interested researchers on different data platforms and their corresponding databases. We have quantified different energy fluxes at the surface of the three measurement sites with permafrost occurrence. Our results show that there are considerable differences in the energy fluxes at the different sites. The energy balance data are particularly important and should be used when interpreting long-term climate

5   related changes of the past as well as to reveal the drivers of past, present and future changes at the individual sites. This is important for modelling approaches as it is showing that not only one single variable such as air temperature alone should be used. Future studies can use the existing data to explore how various permafrost sites will react to the atmospheric warming.

7   Data availability

The data presented and described in this study are available for download at http://dx.doi.org/10.13093/permos-meteo-2021-01

10   (Hoelzle et al., 2021). The data will also be integrated within different databases such as PERMOS or the the Global Energy Balance Archive.

Author contributions. Contribution

MH did the analysis and wrote most of the text, TM, helped with the analysis and created most of the figures, CH, JN, CP and MS helped with creating some figures and writing and interpreting the data.

15   *Acknowledgements.* We want to particularly thank all PERMOS contributers, and to the project participants of the TEMPS project. The study was mainly financed by the University of Fribourg. A special thanks goes to Cathrine Stocker-Mittaz, who started these measurements at the Murtèl-Corvatsch and the Schilthorn sites during her PhD within the PACE project and to Lorenz King and Stephan Gruber who started the measurements at the Stockhorn site. A particular thank goes to Suryanarayanan Balasubramanian who helped with the programming.

References

Arck, M. and Scherrer, D.: A physically based method for correcting temperature data measured by naturally ventilated sensors over snow, Journal of Glaciology, 47, 665–670, doi:https://doi.org/10.3189/172756501781831774, 2001.

Biskaborn, B., Smith, S., Noetzli, J., Matthes, H., Vieira, G., Streletskiy, D., Schoeneich, P., Romanovsky, V., Lewkowicz, T., Abramov, A., Allard, M., Boike, J., Cable, W., Christiansen, H., Delaloye, R., Diekmann, B., Drozdov, D., Etzelmuller, B., Grosse, G., Guglielmin, M., Ingeman-Nielsen, T., Isaksen, K., Ishikawa, M., Johansson, M., Johannsson, H., Joo, A., Kaverin, D., Kholodov, A., Konstantinov, P., Kroger, T., Lambiel, C., Lanckman, J.-P., Luo, D., Malkova, G., Meiklejohn, I., Moskalenko, N., Oliva, M., Phillips, M., Ramos, M., Sannel, A., Sergeev, D., Seybold, C., Skryabin, P., Vasiliev, A., Wu, Q., Yoshikawa, K., Zheleznyak, M., and Lantuit, H.: Permafrost is warming at a global scale, Nature Communications, 10, 469–489, doi:https://doi:10.1038/s41467-018-08240-4, 2019.

Boike, J., Juszak, I., Lange, S., Chadburn, S., Burke, E., Overduin, P. P., Roth, K., Ippisch, O., Bornemann, N., Stern, L., Gouttevin, I., Hauber, E., and Westermann, S.: A 20-year record (1998-2017) of permafrost, active layer and meteorological conditions at a high Arctic permafrost research site (Bayelva, Spitsbergen).

Boike, J., W. C. and Abnizova, A.: Climatology and summer energy and water balance of polygonal tundra in the Lena River Delta, Siberia.

Bowen, I.: The ratio of heat losses by conduction and by evaporation from any water surface, Physical Review, 27, 779–787, 1926.

Brock, B., Willis, I., and Sharp, M.: Measurement and parameterisation of surface roughness variations at Haut Glacier d'Arolla, Journal of Glaciology, 52, 281–297, doi:https://doi.org/10.3189/172756506781828746, 2006.

Brock, B., Mihalcea, C., Kirkbride, M., Diolaiuti, G., Cutler, M., and Smiraglia, C.: Meteorology and surface energy fluxes in the 2005–2007 ablation seasons at the Miage debris-covered glacier, Mont Blanc Massif, Italian Alps, Journal of Geophysical Reserach, 115, doi:https://doi.org/10.1029/2009JD013224, 2010.

Brutsaert, W.: Evaporation Into the Atmosphere: Theory, History and Applications, Springer, New York, 1982.

Burn, C. and Smith, C.: Observations of the 'thermal offset' in near-surface mean annual ground temperatures at several sites near Mayo, Yukon Territory Canada, Arctic, 41, 00–104, 1988.

Chadburn, S., Burke, E., Essery, R., Boike, J., Langer, M., Heikenfeld, M., Cox, P., and Friedlingstein, P.: An improved representation of physical permafrost dynamics in the JULES land-surface model, The Cryosphere, 8, 1493–1508, doi:https://doi.org/10.5194/tc-9-1505-2015, 2015.

Denby, B. and Greuell, W.: The use of bulk and profile methods for determining surface heat fluxes in the presence of glacier winds, Journal of Glaciology, 46, 445–452, doi:https://doi.org/10.3189/172756500781833124, 2000.

Ekici, A., Chadburn, S., Chaudhary, N., Hajdu, L., Marmy, A., Peng, S., Boike, J., Burke, E., Friend, A., Hauck, C., Krinner, G., Langer, M., Miller, P., and Beer, C.: Site-level model intercomparison of high latitude and high altitude soil thermal dynamics in tundra and barren landscapes, The Cryosphere, 9, 1343–1361, doi:https://doi.org/10.5194/tc-9-1343-2015, 2015.

Essery, R., Morin, S., Lejeune, Y., and Ménard, C.: A comparison of 1701 snow models using observations from an alpine site, Advances in Water Resources, 55, 131–148, doi:https://doi.org/10.1016/j.advwatres.2012.07.013, 2013.

Etzelmüller, B.: Recent advances in mountain permafrost research, Permafrost and Periglacial Processes, 24, 99–107, doi:https://doi.org/10.1002/ppp.1772, 2013.

Etzelmüller, B., Guglielmin, M., Hauck, C., Hilbich, C., Hoelzle, M., Isaksen, K., Noetzli, J., Oliva, M., and Ramos, M.: Twenty years of European Mountain Permafrost Dynamics – the PACE Legacy, Environmental Research Letters, 15, 104 070, doi:https://doi.org/10.1088/1748-9326/abae9d, 2020.

Favier, V., Wagnon, P., Chazarin, J.-P., Maisincho, L., and Coudrain, A.: One-year measurements of surface heat budget on the ablation zone of Antizana Glacier 15, Ecuadorian Andes, Journal of Geophysical Reserach, 109, doi:https://doi.org/10.1029/2003JD004359, 2004.

Fiddes, J., Endrizzi, S., and Gruber, S.: Large-area land surface simulations in heterogeneous terrain driven by global data sets: application to mountain permafrost, The Cryosphere, 9, 411–426, doi:https://doi.org/10.5194/tc-9-411-2015, 2015.

5   GCOS: Implementation plan for the global observing system for climate in support of the UNFCCC (2010 update), Report, 2010.

Gruber, S. and Hoelzle, M.: The cooling effect of coarse blocks revisited: a modelling study of a purely conductive mechanism, in: 9th International Conference on Permafrost, Proceedings, edited by Kane, D. and Hinkel, K., vol. 1, pp. 557–561, Institute of Northern Engineering, University of Alaska, 2008.

Haeberli, W. and Beniston, M.: Climate change and its impacts on glaciers and permafrost in the Alps, vol. 27, pp. 258–265, The Royal

10   Swedish Academy of Sciences, 1998.

Hanson, S. and Hoelzle, M.: The thermal regime of the active layer at the Murtèl rock glacier based on data from 2002, Permafrost and Periglacial Processes, 15, 273–282, doi:https://doi.org/10.1002/ppp.499, 2004.

Harris, C., Vonder Mühll, D., Isaksen, K., Haeberli, W., Sollid, J., King, L., Holmlund, P., Dramis, F., Guglielmin, M., and Palacios, D.: Warming permafrost in European mountains, Global and Planetary Change, 39, 215–225, doi:https://doi.org/10.1016/j.gloplacha.2003.04.001,

15   2003.

Hock, R., Rasul, G., Adler, C., Cáceres, B., Gruber, S., Hirabayashi, Y., Jackson, M., Kaeaeb, A., Kang, S., Kutuzov, S., Milner, A., Molau, U., Morin, S., Orlove, B., and Steltzer, H.: High Mountain Areas, vol. 2, p. 202, IPCC, 2019.

Hoelzle, M. and Gruber, S.: Borehole and ground surface temperatures and their relationship to meteorological conditions in the Swiss Alps, in: 9th International Conference on Permafrost. Proceedings, edited by Kane, D. and Hinkel, K., vol. 1, pp. 723–728, Institute of Northern

20   Engineering, University of Alaska, 2008.

Hoelzle, M., Vonder M, D., and Haeberli, W.: Thirty years of permafrost research in the Corvatsch-Furtschellas area, Eastern Swiss Alps: a review, Norwegian Journal of Geography, 56, 137–145, doi:https://doi.org/10.1080/002919502760056468, 2002.

Hoelzle, M., Hauck, C., Mathys, T., Noetzli, J., Pellet, C., and Scherler, M.: Energy balance measurements at three PERMOS sites: Corvatsch, Schilthorn, Stockhorn, doi:http://dx.doi.org/10.13093/permos-meteo-2021-01, 2021.

25   Huggel, C., Fischer, L., Schneider, D., and Haeberli, W.: Research advances on climate-induced slope instability in glacier and permafrost high-mountain environments, Swiss Journal of Geography, 65, 146–156, doi:https://doi.org/10.5194/gh-65-146-2010, 2010.

Huggel, C., Carey, M., Clague, J., and Kääb, A.: The High-Mountain Cryosphere: Changes and Risks, p. 363, Cambridge University Press, 2015.

Imhof, M., Pierrhumbert, G., Haeberli, W., and Kienholz, H.: Permafrost investigation in the Schilthorn massif, Bernese Alps,

30   Switzerland, Permafrost and Periglacial Processes, 11, 189–206, doi:https://doi.org/10.1002/1099-1530(200007/09)11:3<189::AID-PPP348>3.0.CO;2-N, 2000.

IPCC: Climate Change 2013: The Physical Basis. Contribution of working group I to the fifth assessment report of the intergovernmental panel of climate change, Cambridge University Press, Cambridge, United Kingdom and New York, NY, USA, 2013.

Keller, F.: Interaktionen zwischen Schnee und Permafrost. Eine Grundlagenstudie im Oberengadin, Phd thesis, ETH Zurich, Mitteilungen

35   der Versuchsanstalt für Wasserbau, Hydrologie und Glaziologie, 1994.

King, L.: Soil and rock temperatures in discontinuous permafrost: Gornergrat and Unterrothorn, Wallis, Swiss Alps, Permafrost and Periglacial Processes, 1, 177–188, doi:https://doi.org/10.1002/ppp.3430010208, 1990.

Langer, M., Westermann, S., Muster, S., Piel, K., and Boike, J.: The surface energy balance of a polygonal tundra site in northern Siberia - Part 1: Spring to fall, The Cryosphere, 5, 151–171, doi:https://doi.org/10.5194/tc-5-151-2011, 2011a.

Langer, M., Westermann, S., Muster, S., Piel, K., and Boike, J.: The surface energy balance of a polygonal tundra site in northern Siberia - Part 2: Winter, The Cryosphere, 5, 509–524, doi:https://doi.org/10.5194/tc-5-509-2011, 2011b.

5 Luethi, R., Phillips, M., and Lehning, M.: Estimating Non-Conductive Heat Flow Leading to Intra-Permafrost Talik Formation at the Ritigraben Rock Glacier (Western Swiss Alps), Permafrost and Periglacial Processes, 28, 183–194, doi:https://doi.org/10.1002/ppp.1911, 2017.

Marmy, A., Rajczak, J., Delaloye, R., Hilbich, C., Hoelzle, M., Kotlarski, S., Lambiel, C., Noetzli, J., Phillips, M., Salzmann, N., Staub, B., and Hauck, C.: Semi-automated calibration method for modelling of mountain permafrost evolution in Switzerland, The Cryosphere, 10, 10 2693–2719, doi:https://doi.org/10.5194/tc-10-2693-2016, 2016.

Mattson, L. and Gardner, J.: Energy exchange and ablation rates on the debris-covered Rakhiot Glacier, Pakistan, Zeitschrift für Gletscherkunde und Glazialgeologie, 25, 17–32, 1989.

Mellor, M.: Engineering properties of snow, Journal of Glaciology, 19, 15–66, 1977.

Mittaz, C., Hoelzle, M., and Haeberli, W.: First results and interpretation of energy-flux measurements of Alpine permafrost, Annals of 15 Glaciology, 31, 275–280, doi:https://doi.org/10.3189/172756400781820363, 2000.

Mohd Wani, J., J. Thayyen, R., Ojha, C. S. P., and Gruber, S.: The surface energy balance in a cold-arid permafrost environment, Ladakh Himalaya, India, The Cryosphere Discussions, 2020, 1–57, doi:10.5194/tc-2019-286, https://tc.copernicus.org/preprints/tc-2019-286/, 2020.

Moore, R.: On the use of bulk aerodynamic formulae over melting snow, Nordic Hydrology, 14, 193–206, 1983.

20 Munro, D.: Surface roughness and bulk heat transfer on a glacier: Comparison with eddy correlation, Journal of Glaciology, 35, 343–348, 1989.

Nakawo, M. and Young, G.: Estimate of glacier ablation under a debris layer from surface temperature and meteorological variables, Journal of Glaciology, 28, 29–34, 1982.

Nicholson, L. and Benn, D.: Calculating ice melt beneath a debris layer using meteorological data, Journal of Glaciology, 52, 463–470, 25 doi:https://doi.org/10.3189/ 172756506781828584, 2006.

Noetzli, J., Arenson, L., Bast, A., Beutel, J., Delaloye, R., Farinott, D., Gruber, S., Gubler, H., Haeberli, W., Hasler, A., Hauck, C., Hiller, M., Hoelzle, M., Lambiel, C., Pellet, C., Springman, S., Vonder Muehll, D., and Phillips, M.: doi:https:10.3389/feart.2021.607875, Title = Best practice for measuring permafrost temperature in boreholes based on the experience in the Swiss Alps, Journal = Frontiers in Earth Science, Pages = 1-20, Volume = 9, Number = 607875, Year = 2021.

30 Noetzli, J., Christiansen, H., Isaksen, K., Smith, S., Zhao, L., and Streletskiy, D.: Permafrost thermal state, Bulletin of the American Meteorological Society, 101, 34–36, doi:https://doi.org/10.1175/BAMS-D-20-0104.1, 2020.

Nyeki, S., Wacker, S., Aebi, C., Gröbner, J., Martucci, G., and Vuilleumier, L.: Trends in surface radiation and cloud radiative effect at four Swiss sites for the 1996–2015 period, Atmospheric Chemistry and Physics, 19, 13 227–13 241, doi:https://doi.org/10.5194/acp-19-13227-2019, 2019.

35 Ohmura, A.: Objective criteria for rejecting data for bowen ratio flux calculations, Journal of Applied Meteorology, 21, 595–598, doi:https://doi.org/10.1007/s00704-012-0687-x, 1982.

Ohmura, A.: Enhanced temperature variability in high-altitude climate change, Theoretical and Applied Climatology, 110, 499–508, 2012.

Oke, T.: Boundary Layer Climates, Routledge, Nwee York, 2nd edition edn., 1987.

Pellet, C. and Hauck, C.: Monitoring soil moisture from middle to high elevation in Switzerland: Set-up and first results from the SOMO-MOUNT network, Hydrological Earth System Science, 21, 3199–3220, doi:https://doi.org/10.5194/hess-21-3199-2017, 2017.

Pellet, C., Hilbich, C., Marmy, A., and Hauck, C.: Soil moisture data for the validation of permafrost models using direct and indirect measurement approaches at thee alpine sites, Hydrological Earth System Science, 3, doi:https://doi:10.3389/feart.2015.00091, 2016.

5 Pepin, N., Bradley, R., Diaz, H., Baraer, M., Caceres, E., Forsythe, N., Fowler, H., Greenwood, G., Hashmi, M., Liu, X., Miller, J., Ning, L., Ohmura, A., Palazzi, E., Rangwala, I., Schöner, W., Severskiy, I., Shahgedanova, M., Wang, M., Williamson, S., and Yang, D.: Elevation-dependent warming in mountain regions of the world, Nature Climate Change, 5, 424–430, doi:https://doi.org/10.1038/nclimate2563, 2015.

Pepin, N., Arnone, E., Gobiet, A., Haslinger, K., Kotlarski, S., Notarnicola, C., Palazzi, E., Seibert, P., Serafin, S., Sch, W., Terzago, S., Thornton, J., Vuille, M., and Adler, C.: Climate changes and their elevational patterns in the mountains of the world, Reviews of Geophysics, 60, e2020RG000 730, doi:https://doi.org/10.1029/2020RG000730, 2022.

PERMOS: Glaciological Report, Permafrost in Switzerland 2014/2015 to 2017/2018, 16-19, Cryospheric Commission of the Swiss Academy of Sciences, 2019.

Pruessner, L., Phillips, M., Farinott, D., Hoelzle, M., and Lehning, M.: Near-surface ventilation as a key for modelling the thermal regime of coarse blocky rock glaciers, Permafrost and Periglacial Processes, 29, 152–163, doi:https://doi.org/10.1002/ppp.1978, 2018.

Riseborough, D., Shiklomanov, N., Etzelmüller, B., Gruber, S., and Marchenko, S.: Recent advances in permafrost modelling, Permafrost and Periglacial Processes, 19, 137–156, doi:https://doi.org/10.1002/ppp.591, 2008.

Scherler, M., Hauck, C., Hoelzle, M., and Salzmann, N.: Modeled sensitivity of two alpine permafrost sites to RCM-based climate scenarios, Journal of Geophysical Research, doi:https://doi.org/10.1002/jgrf.20069, 2013.

20 Scherler, M., Schneider, S., Hoelzle, M., and Hauck, C.: A two sided approach to estimate heat transfer processes within the active layer of rock glacier Murtèl-Corvatsch, Earth Surface Dynamics, 2, 141–154, doi:https://doi.org/10.5194/esurf-2-141-2014, 2014.

Scherrer, S., Ceppi, P., Croci-Maspoli, M., and Appenzeller, C.: Snow-albedo feedback and Swiss spring temperature trends, Theoretical and Applied Climatology, 110, 509–516, doi:https://doi.org/10.1007/s00704-012-0712-0, 2012.

Sicart, P., Wagnon, P., and Ribstein, P.: Atmospheric controls on the heat balance of Zongo Glacier (16°S, Bolivia), Journal of Geophysical Reserach, 110, doi:https://doi.org/10.1029/2004JD005732, 2005.

Smith, S., O'Neill, H., Isaksen, K., Noetzli, J., and Romanovsky, V.: The changing thermal state of permafrost, Nature Reviews Earth and Environment, 3, doi:https://doi:10.1038/s43017-021-00240-1, 2022.

Sturm, M., Holmgren, J., König, M., and Morris, E.: The thermal conductivity of seasonal snow, Journal of Glaciology, 43, 26–41, 1997.

Takeuchi, Y., Kayastha, R., and Nakawo, M.: Characteristics of ablation and heat balance in debris-free and debris-covered areas on Khumbu Glacier, Nepal Himalayas, in the pre-monsoon season, IAHS Publication, 264, 53–61, 2000.

Walvoord, M. and Kurylyk, B.: Hydrologic impacts of thawing permafrost — A Review, Vadose Zone Journal, 15, 0–20, doi:https://doi.org/10.2136/vzj2016.01.0010, 2016.

Wang, Q., Fan, X., and Wang, M.: Evidence of high-elevation amplification versus Arctic amplification, Science Reports, 2016.

Westermann, S., Luers, J., Langer, M., Piel, K., and Boike, J.: The annual surface energy budget of a high-arctic permafrost site on Svalbard, Norway, The Cryosphere, 3, 245–263, doi:https://doi.org/10.5194/tc-3-245-2009, 2009.

Wicky, J. and Hauck, C.: Numerical modelling of convective heat transport by air flow in permafrost talus slopes, The Cryosphere, 11, 1311–1325, doi:https://doi.org/10.5194/tc-11-1311-2017, 2017.

Wicky, J. and Hauck, C.: Air Convection in the Active Layer of Rock Glaciers, Frontiers in Earth Science, 8, 335, doi:https://doi.org/10.3389/feart.2020.00335, 2020.

Williams, P. and Smith, M.: The Frozen Earth, Cambridge University Press, Nwee York, 1st edition edn., 1989.

WMO: WMO Guidelines on the Calculation of Climate Normals (2010 update), Report 1203, 2017.

5 Wu, Q., Shi, B., and Liu, Y.: Application of models for calculating thermal offset and annual mean permafrost-surface temperature (AMPST) in permafrost research on the Qinghai-Tibet Plateau, in: 8th International Conference on Permafrost, Proceedings, edited by Phillips, M., Springman, S., and Arenson, L., pp. 1247–1252, Swets Zeitlinger, Lisse, Zurich, 2003.
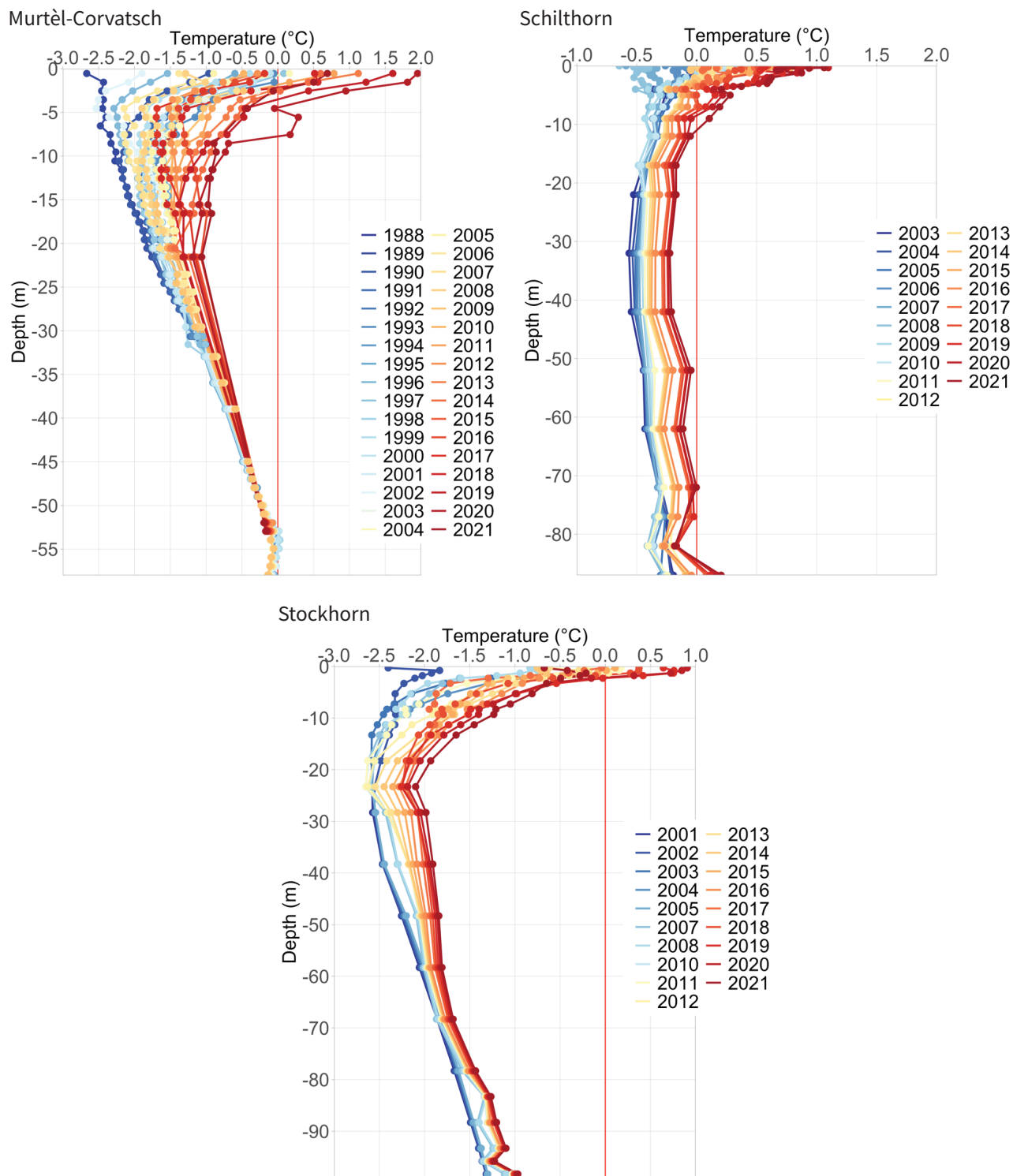
Figure 1. Evolution of borehole temperature measurements over two decades at the three long-term mountain permafrost monitoring sites in the Swiss Alps.
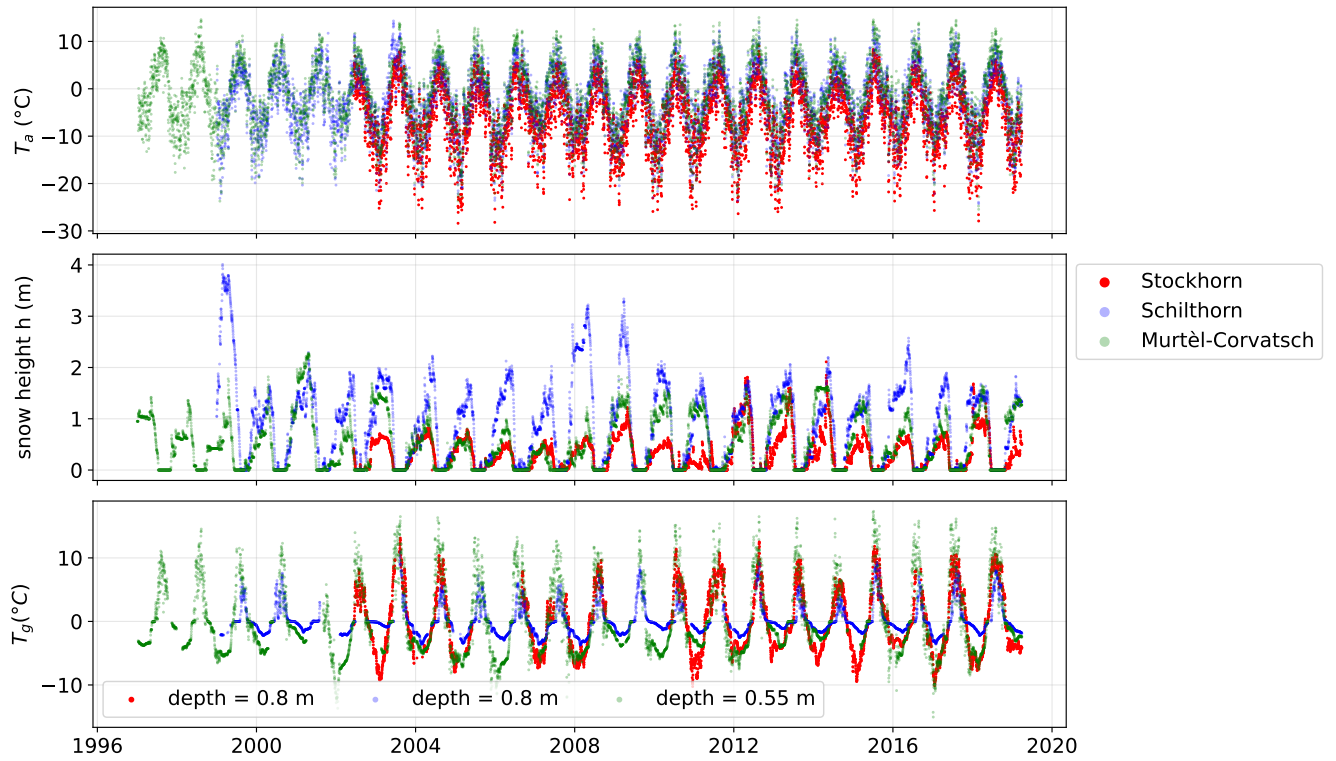
Figure 2. Air temperatures, snow height and ground temperatures for all three stations.
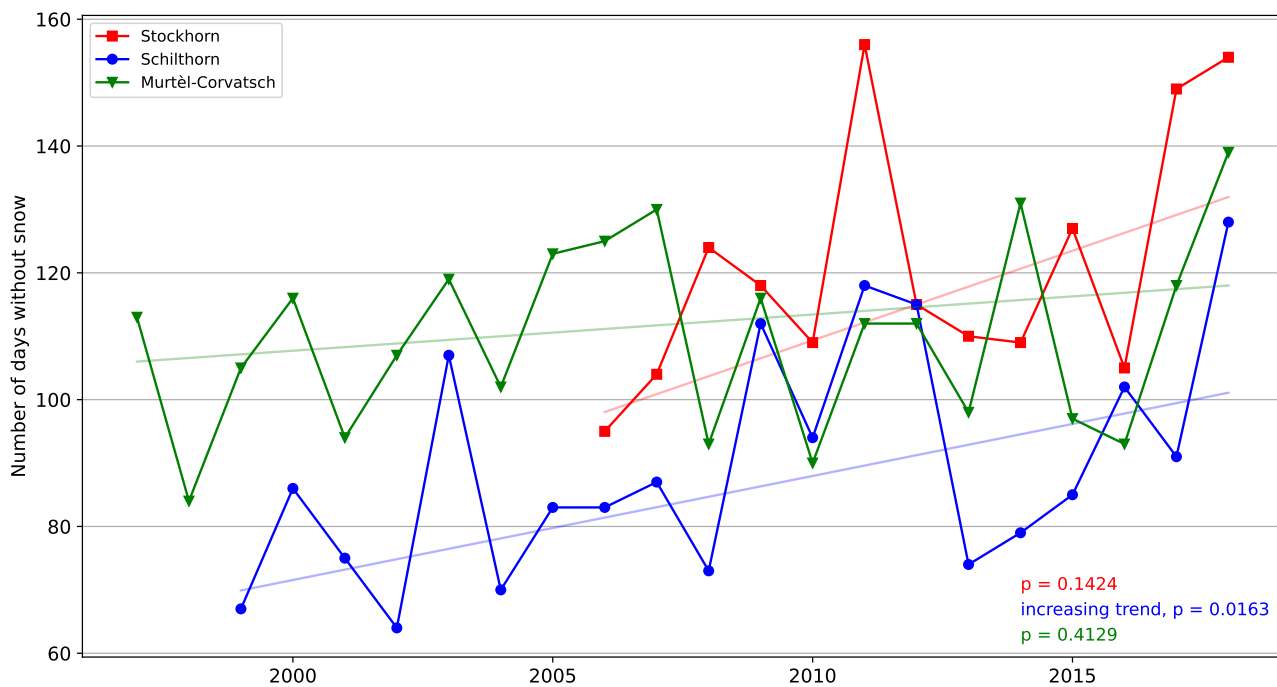
Figure 3. Number of days without snow for the three stations. The tendency to have longer periods without snow is clearly visible.Calculated P values using the Mann-Kendall test show a significant increasing trend in days without snow only for the Schilthorn data (95% confidence interval).
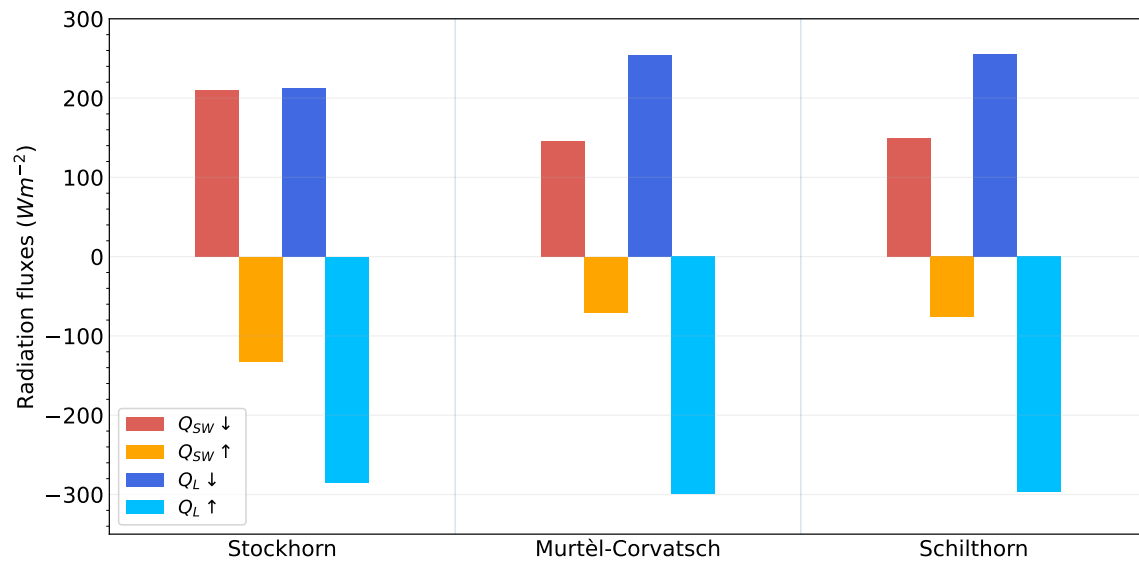
Figure 4. Radiation components for all three stations averaged over the observation periods (Murtèl-Corvatsch (1997 – 2018), Schilthorn (1999 – 2018), Stockhorn (2006 – 2018).
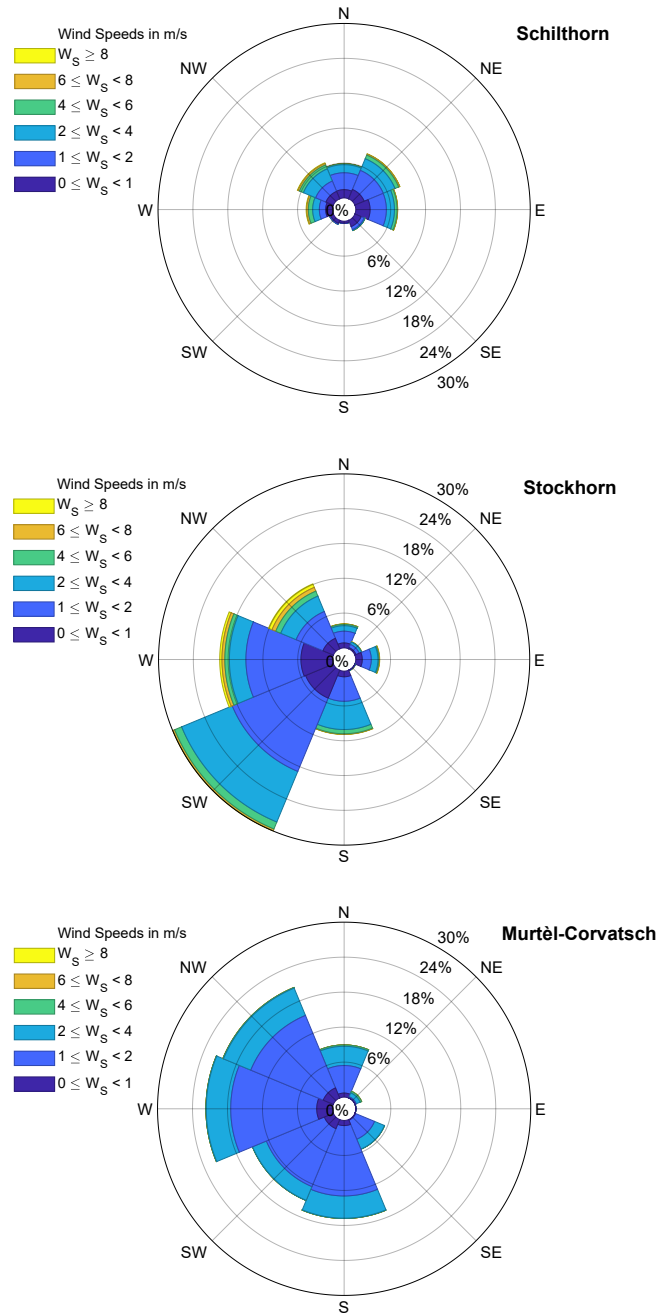
Figure 5. Wind speed and direction at all three stations averaged over the observation periods (Murtèl-Corvatsch (1997 – 2018), Schilthorn (1999 – 2018), Stockhorn (2006 – 2018). Note that scales of relative frequencies are different in the different subplots
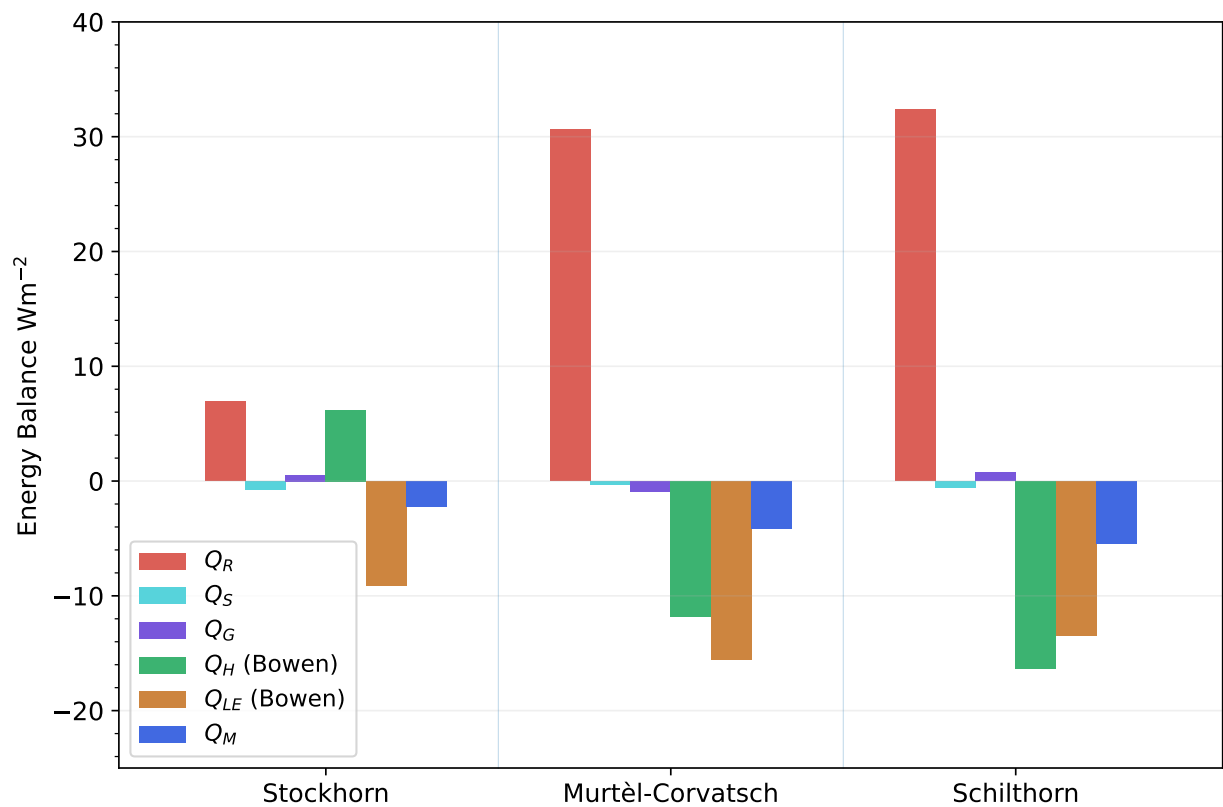
Figure 6. Mean energy balance components for all three stations for the whole observation period (Murtèl-Corvatsch (1997 – 2018), Schilthorn (1999 – 2018), Stockhorn (2006 – 2018).
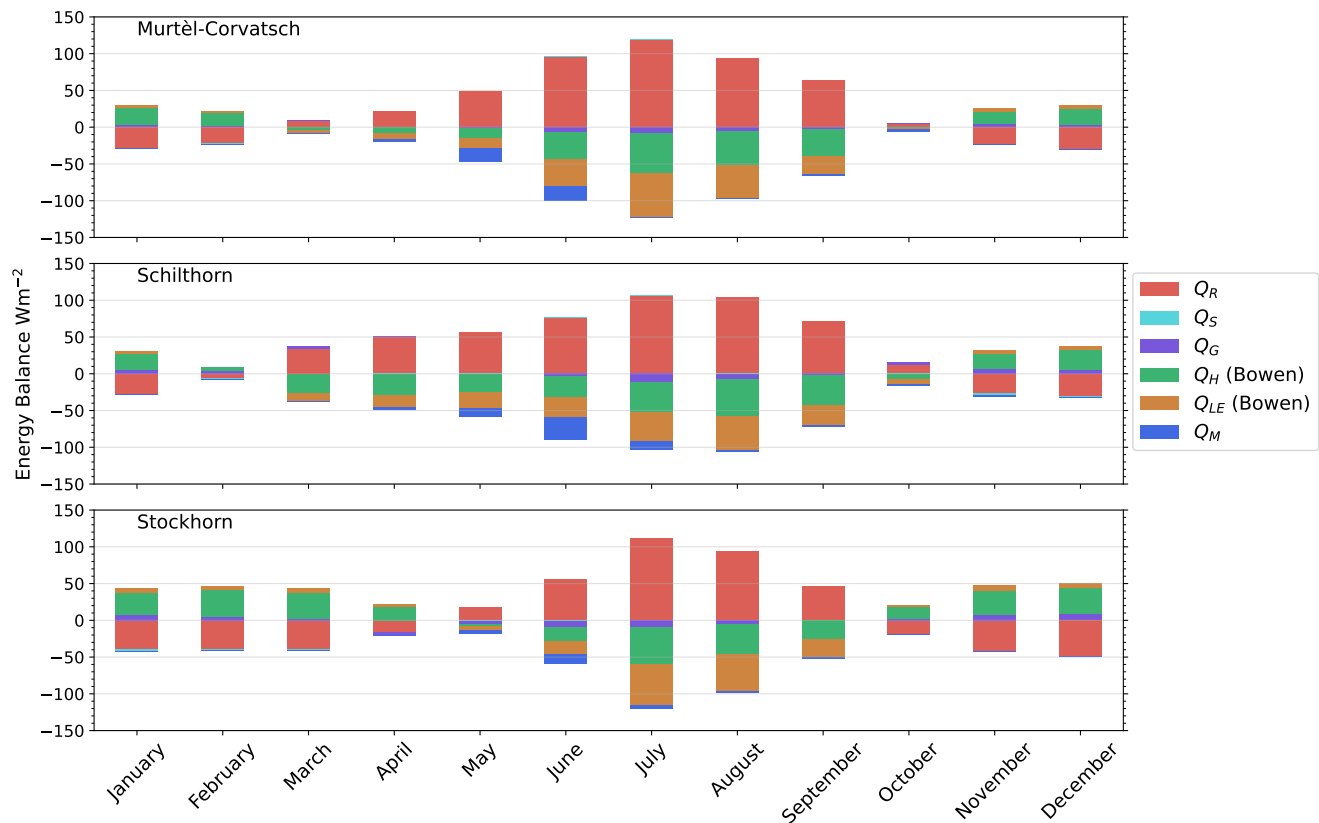
Figure 7. Mean monthly energy balance components for all three stations for the whole observation period (Murtèl-Corvatsch (1997 – 2018), Schilthorn (1999 – 2018), Stockhorn (2006 – 2018).
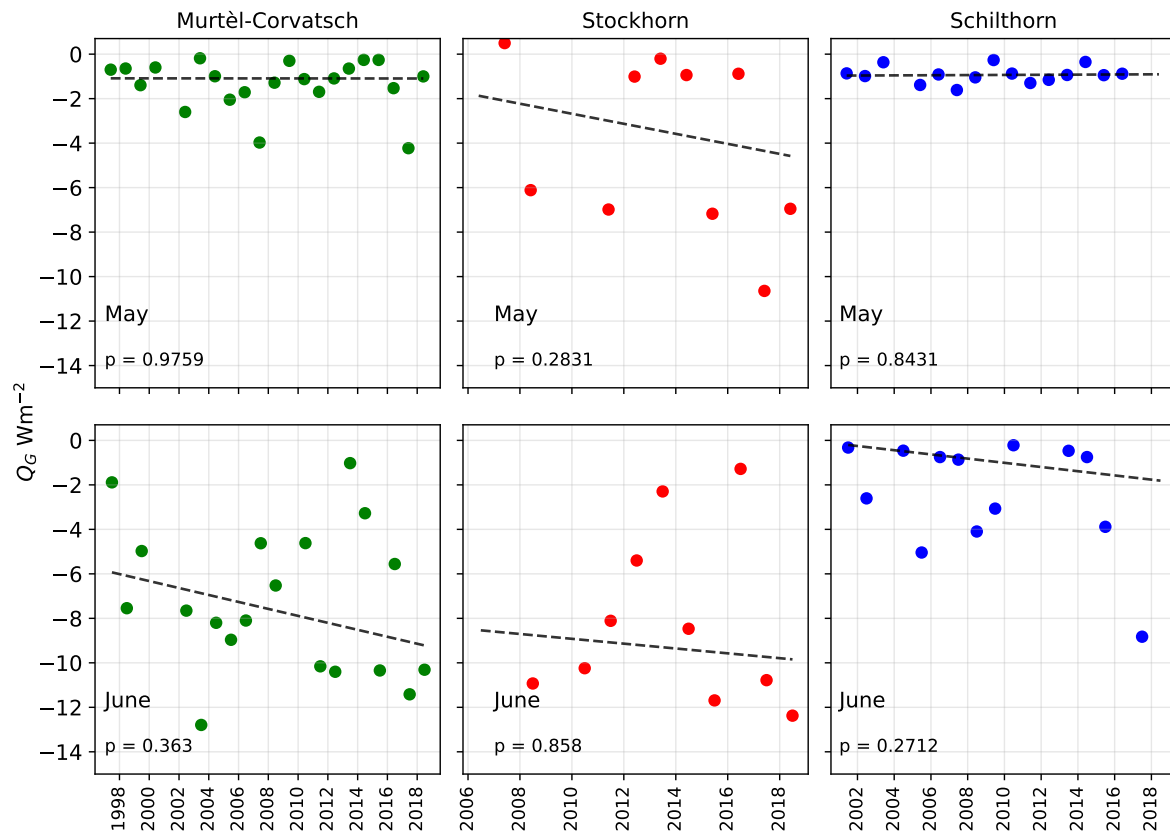
Figure 8. Mean ground heat fluxes for the months May and June for all observation years and for all three stations (Murtèl-Corvatsch (1997 – 2018), Schilthorn (1999 – 2018), Stockhorn (2006 – 2018). P values were calculated using the Mann Kendall test with a 95% confidence interval. The decreasing trends in the plots are statistically non-significant
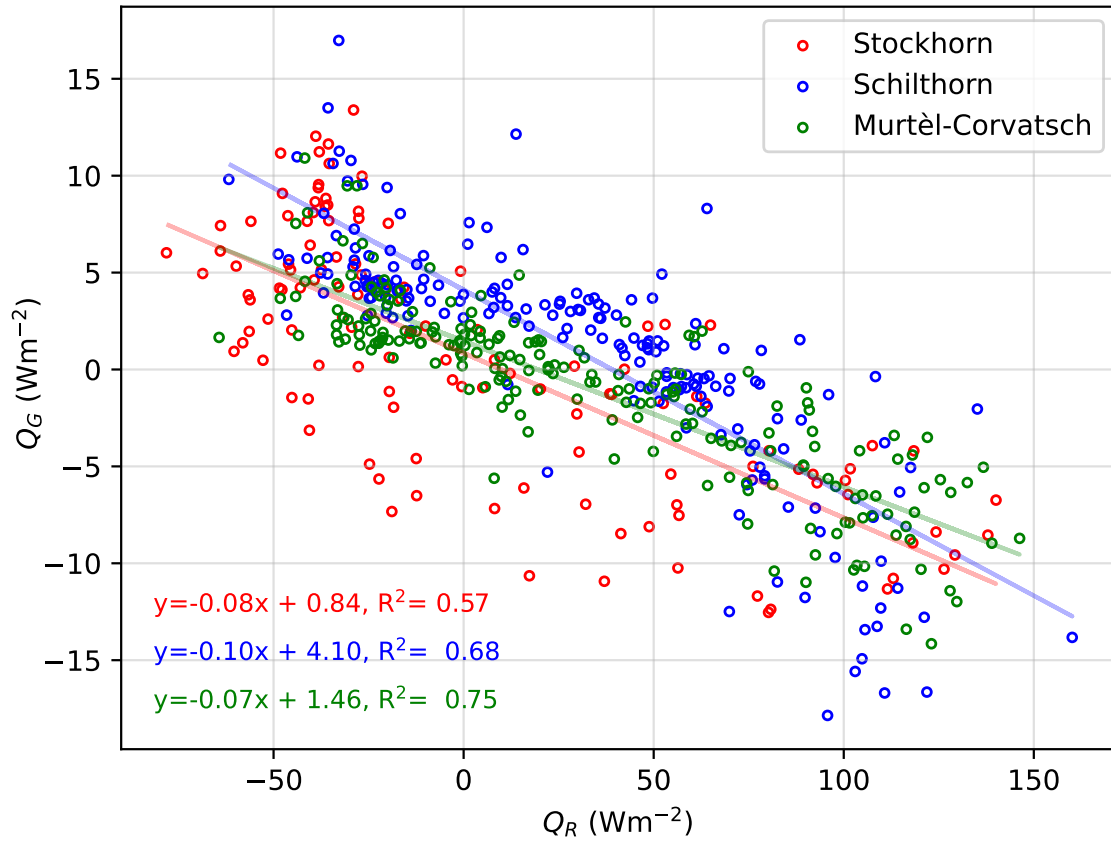
Figure 9. Net radiation versus ground heat flux monthly values for the whole observation periods (Murtèl-Corvatsch (1997 – 2018), Schilthorn (1999 – 2018), Stockhorn (2006 – 2018).
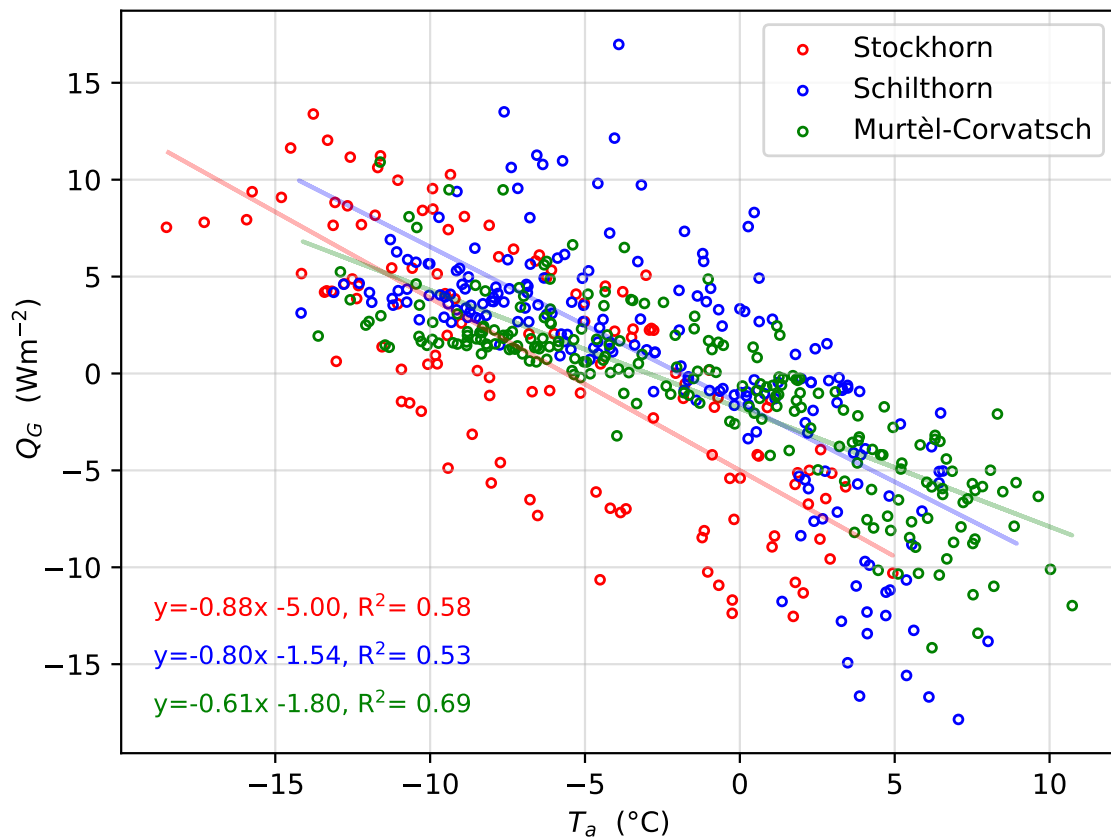
Figure 10. Air temperature versus ground heat flux, monthly values for the whole observation periods (Murtèl-Corvatsch (1997 – 2018), Schilthorn (1999 – 2018), Stockhorn (2006 – 2018).
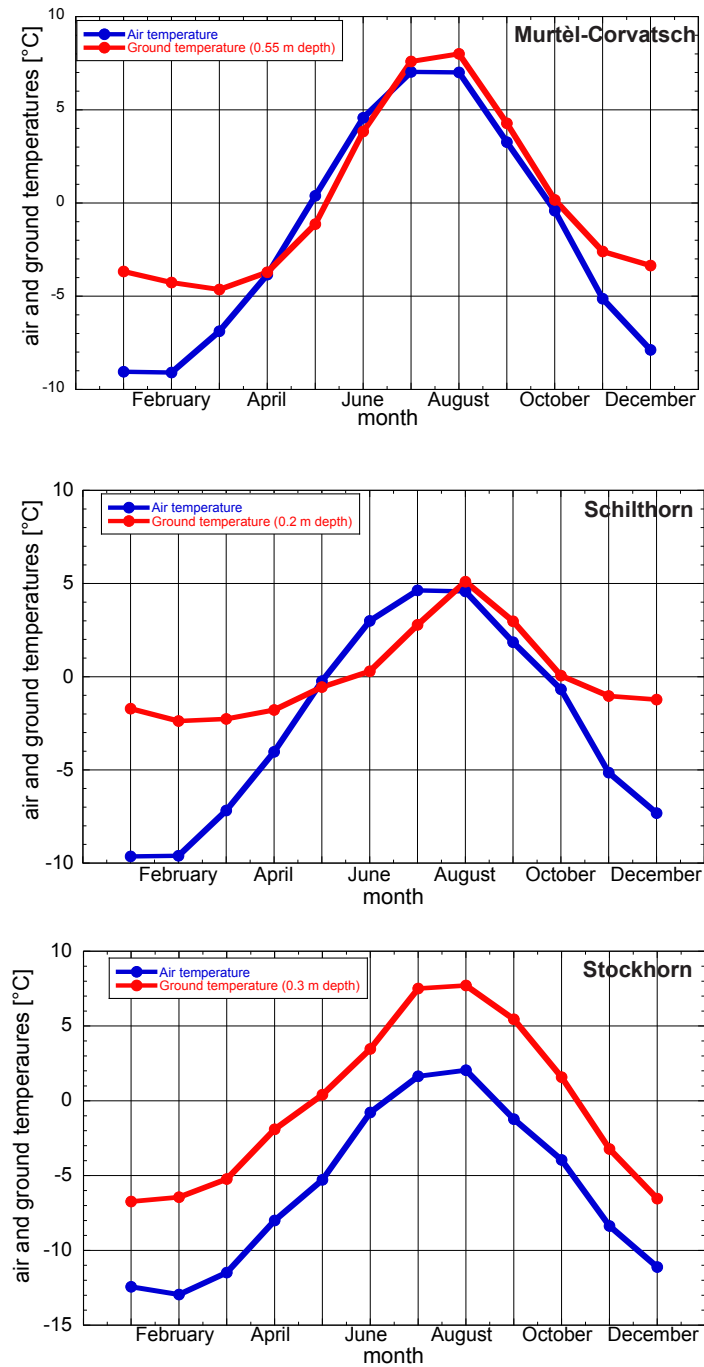
Figure 11. Monthly thermal offsets for all three stations for the whole observation periods (Murtèl-Corvatsch (1997 – 2018), Schilthorn (1999 – 2018), Stockhorn (2006 – 2018).

Table 1. Sensors currently used and their characteristics at the three different sites

variable	sensor (company)	type of sensor	range	accuracy by manufacturer	station
	logger CR10X and CR1000 (Campbell)				
Radiation (short- and longwave)	Netradiometer CNR1 (Kipp&Zonen)	Pyranometer CM3 Pyrgeometer CG3 PT-100 T-sensor	$0.3-3\ \mu m$ $5-50\ \mu m$	$\pm10\%$ for daily total $\pm10\%$ for daily total $\pm10\%$ for daily total	Murtèl-Corvatsch Schilthorn Stockhorn
Air temperature Air humidity	MP-100A Ventilated (Rotronic)	RTD PT-100 C94 hygrometer	$-40-60\,^\circ$C $0-100$ % rh	$\pm10\%$ $\pm2\%$	Murtèl-Corvatsch Schilthorn Stockhorn
Wind speed Wind direction	Model $05103-5$ (Young)	Potentiometer	$0-60\,ms^{-1}$ $0-355\,^\circ$	$\pm0.3\,ms^{-1}$ $\pm3\,^\circ$	Murtèl-Corvatsch Schilthorn Stockhorn
Snow height	SR50 (Campbell)	Ultrasonic electrostatic transducer	$0.5-10$ m	$\pm0.01\,m$	Murtèl-Corvatsch Schilthorn Stockhorn
Surface temperature	Infrared thermometer	Irt/c.5	$-35-60\,^\circ$C	$\pm1.5\,^\circ$C	Murtèl-Corvatsch
Borehole temperature	YSI 44006 (Yellow Springs Instruments) UUB 31J1 (Fenwal)	NTC-thermistors	$-10-40\,^\circ$C	$\pm0.02\,^\circ$C	Murtèl-Corvatsch Schilthorn Stockhorn

Table 2. Information on the linear regression coefficients used for the gap filling of level 2 data (MCH = MeteoSwiss, IMIS = Intercantonal Measurement and Information System)

Murtèl–Corvatsch

Variable	Station used for gap filling	Coefficient a	Coefficient b	Correlation r^2
Air temperature	Corvatsch MCH	1.0322	3.354	0.95
Surface temperature	Murtèl-Corvatsch Air	1.366	-0.896	0.86
Relative humidity	Corvatsch MCH	0.5817	24.109	–
Longwave out	Murtèl-Corvatsch Air	-6.0843	-309.98	0.96
Longwave in	Murtèl-Corvatsch Air	3.9944	260.58	0.78

Schilthorn

Variable	Station used for gap filling	Coefficient a	Coefficient b	Correlation r^2
Air temperature	Schilthorn IMIS1	0.98666	-0.20132	0.97
Relative humidity	Schilthorn IMIS1	0.8889	6.19	0.77
Wind speed	Schilthorn IMIS1	0.2679	0.9511	0.28

Stockhorn

Variable	Station used for gap filling	Coefficient a	Coefficient b	Correlation r^2
Air temperature	Gornergrat MCH	0.97838	-3.847	0.96
Ground temperature	Stockhorn ground temp. 0.3 m	-0.245	1.1379	0.92

Table 3. Mean values and standard deviation for the climate variables calculated based on the mean monthly values and the time period of measurements

	Mean air temperature (°C)	Mean relative humidity (%)	Mean wind speed (ms^{-1})	
Stockhorn	-6.18±5.63	73.20±5.49	2.09±0.57	
Schilthorn	-2.60±5.55	72.73±6.34	1.97±0.48	
Murtèl–Corvatsch	-1.66±6.12	71.69±4.95	1.69±0.32	
	Shortwave incoming radiation (Wm^{-2})	Shortwave outgoing radiation (Wm^{-2})	Longwave incoming radiation (Wm^{-2})	Longwave outgoing radiation (Wm^{-2})
Stockhorn	209.69±82.57	-131.32±64.61	213.35±27.07	-284.78±37.27
Schilthorn	149.61±88.10	-75.87±53.73	254.97±26.72	-296.02±30.05
Murtèl–Corvatsch	147.91±88.21	-71.50±58.79	254.40±27.19	-300.38±38.22
	Mean snow height (m)	Mean ground temperature (°C)	Mean ground temperature (°C)	
Stockhorn	0.32±0.31	-0.43±5.69 (0.3m)	-0.32±4.79 (0.8m)	
Schilthorn	0.87±0.76	0.03±3.03 (0.2m)	0.04±2.66 (0.4m) height	
Murtèl–Corvatsch	0.50±0.50	0.07±5.15 (0.5 m)	-0.28±3.74 (1.5 m)	

Table 4. Mean values and standard deviation for the energy balance components calculated based on the mean monthly values and the time period of measurements

	Mean net radiation balance (Wm^{-2})	Mean melt energy (Wm^{-2})	Mean snow heat flux (Wm^{-2})	Mean ground heat flux (Wm^{-2})
Stockhorn	6.91±57.38	-2.26±5.42	-0.73±0.81	0.51±6.46
Schilthorn	32.40±49.02	-8.46±16.14	-0.52±0.65	0.68±6.08
Murtèl–Corvatsch	30.59±52.62	-4.17±8.85	-0.31±0.45	-0.88±4.56
	Mean sensible heat flux (bulk) (Wm^{-2})	Mean latent heat flux (bulk) (Wm^{-2})	Mean sensible heat flux (Bowen) (Wm^{-2})	Mean latent heat flux (Bowen) (Wm^{-2})
Stockhorn	-7.16±21.91	-8.37±10.23	6.52±23.76	-9.00±22.78
Schilthorn	-6.80±23.63	-6.161±12.695	-13.70±31.25	-13.87±17.54
Murtèl–Corvatsch	-15.28±42.80	-3.43±16.08	-12.26±28.68	-15.67±22.24